Neutron matter at zero temperature with an auxiliary field diffusion Monte Carlo method

A. Sarsa,* S. Fantoni,† and K. E. Schmidt‡
International School for Advanced Studies, SISSA, Trieste, Italy
and INFM DEMOCRITOS National Simulation Center Via Beirut I-34014 Trieste, Italy

F. Pederiva§
Dipartimento di Fisica dell'Università di Trento, Trento, Italy
and INFM DEMOCRITOS National Simulation Center, I-38050 Povo, Trento, Italy
(Received 14 March 2003; published 15 August 2003)

The recently developed auxiliary field diffusion Monte Carlo method is applied to compute the equation of state and the compressibility of neutron matter. By combining diffusion Monte Carlo method for the spatial degrees of freedom and auxiliary field Monte Carlo method to separate the spin-isospin operators, quantum Monte Carlo can be used to simulate the ground state of many-nucleon systems ($A \lesssim 100$). We use a path constraint to control the fermion sign problem. We have made simulations for realistic interactions, which include tensor and spin-orbit two-body potentials as well as three-nucleon forces. The Argonne v_8' and v_6' two-nucleon potentials plus the Urbana or Illinois three-nucleon potentials have been used in our calculations. We compare with fermion hypernetted chain results. We report on the results of a periodic box fermi hypernetted chain calculation, which is also used to estimate the finite size corrections to our quantum Monte Carlo simulations. Our auxiliary field diffusion Monte Carlo (AFDMC) results for v_6 models of pure neutron matter are in reasonably good agreement with equivalent correlated basis function (CBF) calculations, providing energies per particle which are slightly lower than the CBF ones. However, the inclusion of the spin-orbit force leads to quite different results particularly at relatively high densities. The resulting equation of state from AFDMC calculations is harder than the one from previous Fermi hypernetted chain studies commonly used to determine the neutron star structure.

DOI: 10.1103/PhysRevC.68.024308 PACS number(s): 26.60.+c, 21.65.+f, 21.30.Fe, 05.10.Ln

I. INTRODUCTION

The important role played by nucleon-nucleon (N-N) correlations on several properties of dense and cold hadronic matter is a well-established fact [1]. Less established are quantitative studies performed with realistic nuclear interactions derived from N-N data and the spectra of light nuclei. The strong repulsion at short range accompanied with the strong spin-isospin dependence, make *ab initio* calculations of the nuclear matter equation of state one of the most challenging problems in strongly correlated many-body theory.

A theoretical calculation of the nuclear matter energy per particle, as a function of the number density ρ, the temperature T, and the neutron-proton asymmetry $\alpha=(N-Z)/(N+Z)$, with an uncertainty of less than an MeV has become a fundamental issue. On one hand, one would like to use the observational data from neutron stars and supernovae, as well as from heavy-ion collisions, to get information on the many-body nature of the nucleon interaction. On the other hand, it is of interest to understand the effect of N-N correlations, and particularly of those induced by the tensor force, on the structure and the evolution of compact astrophysical objects [2–6].

In this paper we limit ourselves to nonrelativistic model Hamiltonians. Modern two-body potentials [7–9] fit the Nijmegen N-N data [10] below 350 MeV at a confidence level of $\chi^2/N_{data} \sim 1$, and to a large extent give equivalent results for several nuclear and neutron matter properties [11]. However, it has become evident that a two-body potential alone is not sufficient to reproduce the experimental data of nuclei other than the deuteron ($A=2$). In the past few years, the Urbana–Argonne collaboration has produced three-body force models which, when added to the two-body potential, provide a satisfactory fit to the binding energies and the low-lying states of light nuclei with $A \leqslant 10$ [12–14].

It would be desirable to have microscopic calculations of the equation of state of nuclear matter with an accuracy comparable to that of light nuclei or, at least, on the order of the experimental uncertainties of the equilibrium density ρ_0, binding energy per particle at ρ_0, and compressibility. This can be considered as the minimal requirement to attempt the study of hadronic matter at densities larger than ρ_0, and/or with large asymmetries (α close to 1) in a realistic way. Such calculations have to deal necessarily with potentials which are strongly spin-isospin dependent and which include a three-body force.

Most of the microscopic calculations of the nuclear matter equation of state carried out in the past decades have been performed by using perturbation theories based either on ladder diagram summation, such as Brueckner or Green's func-

*Present address: Departamento de Física Moderna, Universidad de Granada, E-18071 Granada, Spain. Electronic address: sarsa@ugr.es
†Electronic address: fantoni@sissa.it
‡Permanent address: Department of Physics and Astronomy, Arizona State University, Tempe, AZ, 85287. Electronic address: kevin.schmidt@asu.edu
§Electronic address: pederiva@science.unitn.it

tion theories [11,15], or correlated basis function theories, based on Fermi hypernetted chain techniques [16–18]. In spite of the important advances made in recent years in the above theories, the required accuracy for the equation of state has not yet been reached.

Quantum Monte Carlo methods have been very successful in calculating the properties of strongly interacting systems in condensed matter physics. They are substantially exact, apart from statistical errors, finite size effects, and the well-known sign problem [19] for Fermi systems. They have been recently used to perform quantum simulations of light nuclei [20,21,14] with modern nonrelativistic Hamiltonians of the type discussed above. However, the exponential growth in the number of spin-isospin states with the number of nucleons A, has kept this method from being applied to larger nuclear systems.

Auxiliary field diffusion Monte Carlo [22] (AFDMC) method has been especially developed to tackle the problem of computing the binding energy of a relatively large nuclear system at the required accuracy. In this approach the particle coordinates are propagated as in standard diffusion Monte Carlo. Auxiliary fields are introduced to uncouple the spin-dependent interaction between particles by means of a Hubbard-Stratonovich transformation. The particle spins only interact with the auxiliary fields which, when integrated, produce the original interaction. The method consists of calculating the auxiliary field integrations by Monte Carlo sampling and then propagating the spin variables. This propagation results in a rotation of each particle's spinor governed by the sampled values of the auxiliary variables. The result is a sampling of the spin variables, which should have less variance than a direct approach where the spins are flipped.

The tensor force couples the spin configurations with the orbital angular momentum so that the wave function becomes complex. The resulting fermion phase problem is handled by applying a path-constraint approximation analogous to the fixed-node approximation. The AFDMC method for the spin-isospin calculations can be viewed as a generalization of the method of Zhang *et al.* [23,24] used in condensed matter lattice systems to the spin-isospin states of nucleon systems, while retaining standard diffusion Monte Carlo method for the spatial degrees of freedom. The AFDMC method has proved to be efficient in dealing with large nucleon systems interacting via semirealistic potentials [22,25,26] and spin-polarized neutron systems [27].

The aim of this paper is to give a detailed description of the AFDMC method and to report on the results for the equation of state of pure neutron matter ($\alpha=1$) with a fully realistic nuclear interaction, at zero temperature. It presents results of AFDMC simulations of 14, 38, 66, and 114 neutrons in a periodic box, interacting via a realistic potential that includes two-body tensor and spin-orbit components, as well as three-body forces. Particular attention is paid to the 14-neutron system, which may serve as a homework problem for different many-body techniques. It is small enough to be handled by traditional quantum Monte Carlo methods [28]. However, it will be shown that the finite size effects of 14 neutron systems are hard to estimate in a realistic way. Actually, results obtained with larger systems (66 or 114 neutrons) show that the equation of state of neutron matter cannot be simulated starting from 14 neutrons in a box, particularly in the high density region. Finite size effects for the larger systems considered here can be fairly well estimated by the recently developed periodic box fermi hypernetted chain (PBFHNC) theory [29]. We have also performed AFDMC calculations of the binding energy of symmetric and asymmetric nuclear matter. A few results obtained with semirealistic spin-dependent central potentials are presented and discussed.

The plan of the paper is the following. The Hamiltonian used in this work is shown in the following section. In Sec. III the problem of the spin degrees of freedom in quantum Monte Carlo simulations is discussed. Section IV is devoted to the description of the AFDMC method, including the calculation of the spin-orbit and the three-body terms of the Hamiltonian. A discussion of the finite size effects along with the periodic box FHNC method is given in Sec. V. The results for the neutron matter equation of state are presented and discussed in Sec. VI. The conclusions and perspectives for the present work are in Sec. VII.

II. THE HAMILTONIAN

We use a nonrelativistic Hamiltonian of the form

$$H=T+V_2+V_3=-\frac{\hbar^2}{2m}\sum_{j=1,N}\nabla_j^2+\sum_{j<k}v_{jk}+\sum_{j<k<l}V_{jkl}, \tag{1}$$

containing the kinetic term, where we have used $\hbar^2/2m=20.735\,54$ MeV fm^2 (which corresponds to the $n-p$ reduced mass), and two- and three-body potentials. The two-body potential belongs to the Urbana-Argonne v_ℓ type,

$$v_\ell=\sum_{j<k}v_{jk}=\sum_{j<k}\sum_{p=1}^{\ell}v_p(r_{jk})O^{(p)}(j,k), \tag{2}$$

where j and k label the two nucleons, r_{jk} is the distance separating the two nucleons, and the spin-isospin–dependent operators $O^p(i,j)$ for $p=1,8$ are given by

$$O^{p=1,8}(j,k)=(1,\vec{\sigma}_j\cdot\vec{\sigma}_k,S_{jk},\vec{L}_{jk}\cdot\vec{S}_{jk})\otimes(1,\vec{\tau}_j\cdot\vec{\tau}_k), \tag{3}$$

where $S_{jk}=3(\hat{r}_{jk}\cdot\vec{\sigma}_j)(\hat{r}_{jk}\cdot\vec{\sigma}_k)-\vec{\sigma}_j\cdot\vec{\sigma}_k$ is the two-nucleon tensor operator, and $\vec{L}_{jk}$ and $\vec{S}_{jk}$ are the relative angular momentum and the total spin, given by

$$\vec{L}_{jk}=\frac{\hbar}{2\imath}(\vec{r}_j-\vec{r}_k)\times(\vec{\nabla}_j-\vec{\nabla}_k), \tag{4}$$

$$\vec{S}_{jk}=\frac{\hbar}{2}(\vec{\sigma}_j+\vec{\sigma}_k). \tag{5}$$

The full Argonne v_{18} potential consists of $\ell=18$ components. Besides the eight components given in Eq. (3), it includes the six $[L^2,\ L^2\ \vec{\sigma}_j\cdot\vec{\sigma}_k,\ (\vec{L}\cdot\vec{S})^2]\ \otimes(1,\vec{\tau}_j\cdot\vec{\tau}_k)$ charge

independent ones, as well as four other charge-symmetry-breaking and charge-dependent terms.

We use a simplified isoscalar version of the v_{18} potential, the so-called v_8' two-body potential [20,30]. This potential contains only the first eight spin-dependent operators in Eq. (3), and equals the isoscalar part of v_{18} in all S and P waves as well as in the $^3D_1$ wave and its coupling to the $^3S_1$. It has been used in a number of Green's function Monte Carlo (GFMC) calculations in light nuclei [20], as well as fermi hypernetted chain at the single operator chain approximation (FHNC/SOC) calculations in nuclear matter [17]; differences with the v_{18} potential give small contributions that can be safely estimated perturbatively or from FHNC/SOC calculations. In the case of pure neutron matter (PNM), the isospin exchange operators are replaced by the identity.

We denote by v_6' the two-body potential model obtained by restricting the v_8' potential to the first six (three for neutron matter) components. Note that this truncation of the Argonne v_8' should not be confused with the recently produced Argonne $AV6'$ potential [31].

The three-body interaction used in our calculations of the equation of state is the Urbana IX potential [20]. For neutrons, the Urbana-IX interaction is given by the sum of a spin-independent and a spin-dependent part,

$$V_{jkl}=V_{jkl}^{SI}+V_{jkl}^{SD}, \tag{6}$$

where

$$V_{jkl}^{SI}=U_0\sum_{cyclic} T^2(m_\pi,c_3;r_{jl})T^2(m_\pi,c_3;r_{lk}),$$

$$V_{jkl}^{SD}=B_{2\pi}\sum_{cyclic}\{X_{jl}^{\pi},X_{lk}^{\pi}\}, \tag{7}$$

and the operator X_{jk}^{π} is given by

$$X_{jk}^{\pi}=Y(m_\pi,c_3;r_{jk})\vec{\sigma}_j\cdot\vec{\sigma}_k+T(m_\pi,c_3;r_{jk})S_{jk}. \tag{8}$$

Notice that in some of our earlier AFDMC calculations we have used $c_3=2.0$ fm^{-2} and $\mu=0.7$ fm^{-1}, as given in the original papers proposing the Urbana-IX potential [32] and the v_8' model interaction [12]. Changing c_3 from 2.0 to 2.1 leads to a $\sim$10% additional increase of the three-body force contribution in neutron matter. In the following, we will denote with $AU8'$ the v_8' plus Urbana-IX interaction, with $AU6'$ the v_6' plus Urbana-IX interaction.

We have also considered the recently developed Illinois three-body potentials, which include two Δ intermediate state diagrams [13], and denoted with IL1, . . . ,IL4.

III. SPIN DEGREES OF FREEDOM

Standard Green's function or diffusion Monte Carlo methods for central potentials sample only the particle positions since the spin or isospin of the particles can be fixed. The Green's function Monte Carlo method used in light nuclei also samples the particle positions, but a complete description of the spin degrees of freedom is kept for each sample position leading to an exponential growth of the number of spin-isospin states with particle number A. This exponential behavior can be removed by sampling rather than summing the spin-isospin degrees of freedom.

We define a walker to be the $3A$ coordinates of the A particles and A spinors each giving the four amplitudes for a particle to be in the proton-up, proton-down, neutron-up, and neutron-down states. For the special case where walkers are sampled from the usual neutron-proton up-down basis, the spinors would be one of (1,0,0,0), (0,1,0,0), (0,0,1,0), and (0,0,0,1) for each particle. Our auxiliary field method requires the more general definition as shown below.

As usual, the overlap of the walker bra with the trial ket is the wave function amplitude,

$$\langle R,S|\Psi_T\rangle\equiv\Psi_T(R,S). \tag{9}$$

Direct sampling of the spin-isospin in the usual spin-up/-down basis requires a good trial function that can be evaluated efficiently. This can be most easily seen for the variational formalism, but the same analysis applies to Green's function or diffusion Monte Carlo formalism. A variational Monte Carlo calculation can be formulated by minimizing the expectation value of the Hamiltonian,

$$\langle H\rangle=\frac{\langle\Psi_T|H|\Psi_T\rangle}{\langle\Psi_T|\Psi_T\rangle}=\frac{\int dR\sum_{S,S'}\Psi_T^*(R,S')H_{S',S}\Psi_T(R,S)}{\int dR\sum_S|\Psi_T(R,S)|^2}, \tag{10}$$

where for a v_6 interaction we would have

$$H_{S',S}=\langle S'|S\rangle\left[-\frac{\hbar^2}{2m}\sum_n\nabla_n^2\right]+\langle RS'|V|RS\rangle, \tag{11}$$

with a straightforward generalization for spin-orbit terms.

Variational Monte Carlo calculation can be implemented with either spin sums [33–35],

$$\langle H\rangle=\int dR E_L(R)P(R),$$

$$P(R)=\frac{\sum_S|\Psi_T(R,S)|^2}{\int dR\sum_S|\Psi_T(R,S)|^2},$$

$$E_L(R)=\frac{\sum_{S,S'}\Psi_T^*(R,S')H_{S',S}\Psi_T(R,S)}{\sum_S|\Psi_T(R,S)|^2}, \tag{12}$$

or spin samples [36],

$$\langle H\rangle = \int dR \sum_S E_L(R,S)P(R,S),$$

$$P(R,S) = \frac{|\Psi_T(R,S)|^2}{\int dR \sum_S |\Psi_T(R,S)|^2},$$

$$E_L(R,S) = \frac{\sum_{S'} \Psi_T^*(R,S')H_{S',S}\Psi_T(R,S)}{|\Psi_T(R,S)|^2}. \quad (13)$$

In these equations, P is the probability density to be sampled and E_L is the local energy. A typical variational calculation would use the Metropolis algorithm to sample either R or R and S from P, and average the value of the local energy over these samples.

Notice that for an eigenstate of H, both $E_L(R,S)$ and $E_L(R)$ are constant. So, as for central potentials, the variance will be low if the trial function is accurate. Also note that the spin sum S' in the definition of $E_L(R,S)$ is polynomial rather than exponential in A. For example, a pair potential will have only order A^2 terms where two particles have different spin-isospins.

The variance per sample for complete spin sums will be lower than for spin samples. However, since the spin sums grow exponentially with particle number, spin sampling should be more efficient for large particle number if the trial function can be evaluated efficiently for a single many-particle spin state S.

Unfortunately, all of the good trial wave functions currently used for large numbers of particles cannot be evaluated efficiently for a single many-particle spin state S. For example light nuclei variational Monte Carlo calculations are typically done using a pair product (or more complicated) wave function,

$$|\Psi_P\rangle = \mathcal{S}\prod_{j<k} f_{jk}^c \left[1 + \sum_p u_{jk}^p O_{jk}^p\right]|\Phi\rangle, \quad (14)$$

where $\mathcal{S}$ symmetrizes the operator products, and $|\Phi\rangle$ is the antisymmetric model state. While the symmetrizer produces all possible orderings of the operators and therefore gives $\mathcal{O}(A^2!)$ terms, normally the commutator terms are fairly small and the ordering of the operators is sampled. However, even within a fixed ordering, each operator in the product term when operating on a single many-particle spin-isospin state will produce four or eight new states depending on whether isospin exchange gives a new state. $\mathcal{O}(A)$ operators out of the $\mathcal{O}(A^2)$ total acting on a single state are enough to populate all the states. Therefore a straightforward evaluation of $\langle RS|\Psi_P\rangle$ for this wave function will have the same computational complexity as evaluating a complete set of spin-isospin states at the position R. Since computing all the states have the same cost as a single state, full spin sums are used for these calculations.

If good trial functions for spin-isospin–dependent interactions can be devised which can be evaluated or sampled efficiently at a single many-particle space position and spin-isospin state, straightforward generalizations of standard central potential Monte Carlo methods, both variational and Green's function, with spin-state sampling will solve the nuclear many-particle Hamiltonian.

IV. THE AFDMC METHOD

Since direct evaluation of the pair product wave function is not computationally feasible for large numbers of particles, and so far we have no good methods of sampling these wave functions, we instead drop the operator terms altogether and sample the spin-isospin variables using a rather poor, but easy to evaluate, wave function. Since this wave function does not contain amplitudes of the spin states of the correct solution, we cannot use it to sample the spins. Instead, we rewrite the propagator as an integral over auxiliary fields using the Hubbard-Stratonovich transformation,

$$e^{-(1/2)\lambda O^2\Delta t} = \frac{1}{\sqrt{2\pi}}\int_{-\infty}^{\infty} dx e^{-x^2/2} e^{x\sqrt{-\lambda\Delta t}O}, \quad (15)$$

where O can be a one-body operator. To make use of this transformation we write our propagator as the left-hand side of Eq. (15), so that the integrand of the right-hand side is a product of one-body terms. The integrand has a form such that propagating a walker at $|R,S\rangle$ results in another walker of the same form at $|R',S'\rangle$.

For N neutrons, the v_6 two-body interaction can be split into two parts,

$$\sum_{j<k} v_{jk} = B + \frac{1}{2}\sum_{j,\alpha,k,\beta} \sigma_{j,\alpha} A_{j,\alpha;k,\beta}\ \sigma_{k,\beta}, \quad (16)$$

where roman subscripts j and k are particle labels while greek subscripts α and β are cartesian components. The matrix A and the scalar B are functions of the particle positions,

$$B = \sum_{j<k} [v_1(r_{jk}) + v_2(r_{jk})],$$

$$A_{j,\alpha;k,\beta} = [v_3(r_{jk}) + v_4(r_{jk})]\delta_{\alpha\beta} + [v_5(r_{jk}) + v_6(r_{jk})] \times [3\hat{r}_{jk}\cdot\hat{x}_\alpha \hat{r}_{jk}\cdot\hat{x}_\beta - \delta_{\alpha\beta}]. \quad (17)$$

$A_{j,\alpha;k,\beta}$ is taken to be zero when $j=k$. A can be viewed as a $3N$ by $3N$ real symmetric matrix. It therefore has real eigenvalues and eigenvectors defined by

$$\sum_{k,\beta} A_{j,\alpha;k,\beta}\psi_n^{k\beta} = \lambda_n \psi_n^{j\alpha}. \quad (18)$$

The potential can be written as

$$\sum_{j<k} v_{jk} = B + \frac{1}{2}\sum_{j,\alpha,k,\beta,n} \sigma_{j\alpha}\psi_n^{j\alpha}\lambda_n\sigma_{k\beta}\psi_n^{k\beta} = B + \frac{1}{2}\sum_{n=1}^{3A} (O_n)^2\lambda_n, \quad (19)$$

with

$$O_n = \sum_{j\alpha} \sigma_{j\alpha} \psi_n^{j\alpha}. \tag{20}$$

Each of the O_n is a sum of one-body operators as required above.

After applying the Hubbard-Stratonovich transformation, the short time approximation for the propagator can be written as

$$\left(\frac{m}{2\pi\hbar^2\Delta t}\right)^{3A/2} \exp\left(-\frac{m|R-R'|^2}{2\hbar^2\Delta t}\right) e^{-B(R)\Delta\tau} \times \prod_n \frac{1}{\sqrt{2\pi}} \int_{-\infty}^{\infty} dx_n e^{-x_n^2/2} e^{x_n\sqrt{-\lambda_n\Delta t}O_n}. \tag{21}$$

The O_n do not commute, so we need to keep the time steps small so that the commutator terms can be ignored.

We sample a value of x for each of the $3A$ auxiliary field variables. Once these values are known, the propagation reduces to a rotation in the spin space, and, therefore, to multiplying the current spinor value for each particle by the set of matrices given by the transformation above. For a given eigenvalue $\lambda_n \leqslant 0$ in Eq. (19), the spin states of particle k, $|\eta_k'\rangle = a_k'|\uparrow\rangle + b_k'|\downarrow\rangle$, will be rotated to the new one $|\eta_k\rangle$ having the following components:

$$\begin{aligned} a_k &= a_k'[\cosh(\alpha_n) + \sinh(\alpha_n)\psi_n^z(k)] \\ &\quad + b_k' \sinh(\alpha_n)[\psi_n^x(k) - \imath\psi_n^y(k)], \\ b_k &= b_k'[\cosh(\alpha_n) - \sinh(\alpha_n)\psi_n^z(k)] \\ &\quad + a_k' \sinh(\alpha_n)[\psi_n^x(k) + \imath\psi_n^y(k)], \end{aligned} \tag{22}$$

where

$$\alpha_n = \Delta t|\lambda_n| x_n \sqrt{[\psi_n^x(k)]^2 + [\psi_n^y(k)]^2 + [\psi_n^z(k)]^2}, \tag{23}$$

and x_n is the sampled Hubbard–Stratonovich value. For positive values of λ_n, one has a similar set of equations, in which $\sinh(\alpha_n)$ is substituted with $\imath \sin(-\alpha_n)$.

Finally, it is worth mentioning here that importance sampling has been used for the integral in the Hubbard-Stratonovich (HS) variables. The value of the overlap of the walker with the trial function will not be peaked around $x_n = 0$, but will be shifted. Rather than sampling from the gaussian we preferentially sample values where we predict the trial function will be larger. One way is to shift the sampled Gaussian, values with a drift term analogous to the drift term in diffusion Monte Carlo one by replacing the σ operators by their expectation value at the current R,S value and taking the real part. That is, we write

$$\begin{aligned} &\frac{1}{\sqrt{2\pi}} \int_{-\infty}^{\infty} dx_n e^{-x_n^2/2} e^{x_n\sqrt{-\lambda_n\Delta t}O_n}, \\ &= \frac{1}{\sqrt{2\pi}} \int_{-\infty}^{\infty} dx_n e^{-(x_n-\bar{x}_n)^2/2} e^{x_n\sqrt{-\lambda_n\Delta t}O_n} e^{-2\bar{x}_n x_n + \bar{x}_n^2/2}, \\ &\bar{x}_n = \mathrm{Re}[\sqrt{-\lambda_n\Delta t}\ \langle O_n\rangle], \\ &\langle O_n\rangle = \frac{\langle\Psi_T|O_n|R,S\rangle}{\langle\Psi_T|R,S\rangle}, \end{aligned} \tag{24}$$

and sample the shifted Gaussian; the last correction term is included in the weight. With this real shift and the compensating weight, only the efficiency of the algorithm is changed. We have tried other schemes using a discretized Gaussian integration with altered probabilities and compensating weights with very little difference in the overall efficiency. In Ref. [37] a complex drift rather than the real drift in Eq. (24) has been used. Unlike our real drift above, this can change based on how the path constraint is applied.

A. Three-body potential

For a neutron system, the spin-dependent part of Urbana-IX potential, given in Eqs. (6) and (7), reduces to a sum of terms containing only two-body spin operators but with a form and strength that depends on the positions of three particles. As will be seen below, for a fixed position of the particles, the inclusion of three-body potentials of the Urbana-IX type in the Hamiltonian does not add any additional complications. It simply changes the strength of the coefficients of the terms in the potential and can be trivially incorporated in the AFDMC calculations.

The anticommutator in Eq. (7) can be written as

$$\{X_{jl}^{\pi}, X_{lk}^{\pi}\} = 2\ x_{jkl}^{\mu\nu}\sigma_j^{\mu}\sigma_k^{\nu}, \tag{25}$$

where

$$x_{jkl}^{\mu\nu} = y_{jl}y_{lk}\delta_{\mu\nu} + y_{jl}t_{lk}^{\mu\nu} + t_{jl}^{\mu\nu}y_{lk} + t_{jl}^{\mu\alpha}t_{lk}^{\alpha\nu}, \tag{26}$$

and

$$\begin{aligned} y_{jl} &= Y(m_\pi, c_3, r_{jl}) - T(m_\pi, c_3, r_{jl}), \\ t_{jl}^{\mu\nu} &= 3T(m_\pi, c_3, r_{jl})\hat{r}_{jl}^{\mu}\hat{r}_{jl}^{\nu}. \end{aligned} \tag{27}$$

The spin-dependent (SD) part of the three-body interaction V_3^{SD} can then be easily incorporated in the matrix $A_{j,\alpha,k,\beta}$ of Eq. (17), by the following substitution:

$$A_{j,\alpha;k,\beta} \rightarrow A_{j,\alpha;k,\beta} + 2\sum_l B_{2\pi} x_{jkl}^{\alpha\beta}. \tag{28}$$

Similarly, the new terms in the Illinois potentials can be included into this matrix.

B. The spin-orbit propagator

A first-order approximation [21] to the spin-orbit contribution to the propagator can be obtained by operating the derivative appearing in the $\vec{L}_{jk}\cdot\vec{S}_{jk}$ operator on the free propagator G_0,

$$(\vec{\nabla}_j-\vec{\nabla}_k)G_0(R,R')=-\frac{m}{\hbar^2\Delta t}(\Delta\vec{r}_j-\Delta\vec{r}_k)G_0(R,R'), \tag{29}$$

and substituting this expression back into the propagator. As a result, the spin-orbit part P_{LS} of the propagator is factored out and is finally written as

$$\begin{aligned}P_{LS}&=\exp\left(\sum_{j\neq k}\frac{mv_{LS}(r_{jk})}{4\imath\hbar^2}[\vec{r}_{jk}\times(\Delta\vec{r})_{jk}]\cdot\vec{\sigma}_j\right)\\&=\exp\left(\sum_{j\neq k}\frac{mv_{LS}(r_{jk})}{4\imath\hbar^2}(\vec{\Sigma}_{jk}\times\vec{r}_{jk})\cdot\Delta\vec{r}_j\right),\end{aligned} \tag{30}$$

where $(\Delta\vec{r})_{jk}=\Delta\vec{r}_j-\Delta\vec{r}_k$ and $\vec{\Sigma}_{jk}=\vec{\sigma}_j+\vec{\sigma}_k$.

However, a careful analysis of the above expressions show that they include some spurious contributions linear in Δt. In order to see this the wave function is expanded, as usual, in the integral form of the imaginary time Schrödinger equation keeping only linear terms,

$$\begin{aligned}\Psi(R)=&\Delta t\left[\frac{1}{2m}\sum_j\nabla_j^2-V+E_0\right]\Psi(R)\\&+\int dR'G_0(R,R')P_{LS}\left[\Psi(R)-\sum_p\Delta\vec{r}_p\cdot\vec{\nabla}_p\Psi(R)\right]\\&+\cdots.\end{aligned} \tag{31}$$

At this point, P_{LS} is expanded by using the second form of this propagator given in Eq. (30) keeping both linear and quadratic terms in $\Delta\vec{r}$. The integral in R' can be done by taking into account that (i) the Gaussian factor integrates to 1 if there are no powers of $\Delta\vec{r}$, (ii) terms containing only one power of a $\Delta\vec{r}$ integrate to zero, (iii) quadratic terms containing powers of different components of $\Delta R'$ integrate to zero, and (iv) terms like $(\Delta x_j')^2$ integrate to $\Delta t\hbar^2/m$.

We first consider the part coming from the linear terms in $\Delta\vec{r}$ in both the wave function and P_{LS}. These terms after integration give

$$-\Delta t\sum_{j\neq k}\frac{v_{LS}(r_{jk})}{4\imath}[(\vec{\sigma}_j+\vec{\sigma}_k)\times\vec{r}_{jk}]\cdot\vec{\nabla}_j\Psi(R). \tag{32}$$

The expression above can be further simplified by interchanging the dummy indices j and k,

$$-\Delta t\sum_{j<k}v_{LS}(r_{jk})[\vec{L}\cdot\vec{S}]_{jk}\Psi(R), \tag{33}$$

which is the spin-orbit contribution to the Hamiltonian multiplied by $-\Delta t$.

However, the P_{LS} propagator includes other terms which are of the same order in Δt. They come from the quadratic $\Delta\vec{r}$ terms of the expansion of P_{LS},

$$\begin{aligned}\Delta t(V_2+V_3)=&\Delta t\frac{m}{32}\sum_j\sum_{k\neq j}\sum_{p\neq j}v_{LS}(r_{jk})v_{LS}(r_{jp})\\&\times(\vec{\Sigma}_{jk}\times\vec{r}_{jk})\cdot(\vec{\Sigma}_{jp}\times\vec{r}_{jp})\\=&\Delta t\frac{m}{32\hbar^2}\sum_j\sum_{k\neq j}\sum_{p\neq j}v_{LS}(r_{jk})v_{LS}(r_{jp})\\&\times\{\vec{r}_{jk}\cdot\vec{r}_{jp}\vec{\Sigma}_{jk}\cdot\vec{\Sigma}_{jp}-\vec{\Sigma}_{jp}\cdot\vec{r}_{jk}\vec{\Sigma}_{jk}\cdot\vec{r}_{jp}\}.\end{aligned} \tag{34}$$

The terms with $k=p$ give rise to a two-body additional effective potential $V_2^{add}=-V_2$,

$$V_2^{add}=-\sum_{j<k}\frac{mr_{jk}^2v_{LS}^2(r_{jk})}{8\hbar^2}[2+\vec{\sigma}_j\cdot\vec{\sigma}_k-\vec{\sigma}_j\cdot\hat{r}_{jk}\vec{\sigma}_k\cdot\hat{r}_{jk}]. \tag{35}$$

The terms with $k\neq p$ lead to a three-body additional effective potential $V_3^{add}=-V_3$, given by

$$\begin{aligned}V_3^{add}=&-\sum_{j<k<p}\sum_{\text{cyclic}}\frac{mr_{jk}r_{jp}v_{LS}(r_{jk})v_{LS}(r_{jp})}{16\hbar^2}\\&\times\{\hat{r}_{jk}\cdot\hat{r}_{jp}[2+\vec{\sigma}_k\cdot\vec{\sigma}_j+\vec{\sigma}_p\cdot\vec{\sigma}_j+\vec{\sigma}_k\cdot\vec{\sigma}_p]\\&-\vec{\sigma}_j\cdot\hat{r}_{jk}\vec{\sigma}_k\cdot\hat{r}_{jp}-\vec{\sigma}_p\cdot\hat{r}_{jk}\vec{\sigma}_j\cdot\hat{r}_{jp}-\vec{\sigma}_p\cdot\hat{r}_{jk}\vec{\sigma}_k\cdot\hat{r}_{jp}\}.\end{aligned} \tag{36}$$

Therefore in the actual propagation it is necessary to include explicitly these terms with opposite sign if one is using P_{LS} as given by Eq. (30).

An alternative method that we have also used comes from realizing that the counterterms are produced by the next order term in the series expansion of the exponential. These terms either average to zero, or are higher order in the time step or give incorrect contributions. Subtracting them gives the propagator,

$$\begin{aligned}&\exp\left(\sum_{j\neq k}\frac{mv_{LS}(r_{jk})}{4\imath\hbar^2}[\vec{r}_{jk}\times(\Delta\vec{r})_{jk}]\cdot\vec{\sigma}_j\right)\\&\times\exp\left(-\frac{1}{2}\left[\sum_{j\neq k}\frac{mv_{LS}(r_{jk})}{4\imath\hbar^2}[\vec{r}_{jk}\times(\Delta\vec{r})_{jk}]\cdot\vec{\sigma}_j\right]^2\right),\end{aligned} \tag{37}$$

with the second exponential giving the required counter terms to include. The two forms are equivalent to first order in Δt.

C. Trial wave function

In our calculations we use the simple trial function given by a Slater determinant of one-body space-spin orbitals multiplied by a central Jastrow correlation,

$$|\Psi_T\rangle = \left[\prod_{j<k} f(r_{jk})\right] \mathcal{A}\left[\prod_j \left|\phi_j, s_j\right\rangle\right], \tag{38}$$

where $\mathcal{A}$ is the antisymmetrizer of A particles. The overlap of a walker with this wave function is the determinant of the space-spin orbitals, evaluated at the walker position and spinor for each particle (for nuclear matter the spinor also includes the isospin), and multiplied by a central Jastrow product.

For unpolarized neutron matter in a box of side L, the orbitals are plane waves that fit in the box times up and down spinors. The usual closed shells are 2, 14, 38, 54, 66, 114, . . . for neutrons and 4, 28, 76, . . . for nucleons.

The Jastrow correlation function $f(r)$ has been taken as the first component of the FHNC/SOC correlation operator $\hat{F}_{ij}$, which minimizes the energy per particle of either neutron or nuclear matter at the desired density [16] (see also Sec. V).

As noted in Sec. III, a trial function with spin exchange and tensor correlations requires exponentially increasing computational work as the number of particles increases. The advantages of our trial function is that it is totally antisymmetric, and for A particles requires order A^3 operations to evaluate. However, it does not contain any amplitude generated by the tensor force where spins are flipped with a compensating orbital angular momentum. It is left to the AFDMC method to generate these missing components.

Other forms of a trial wave function can be used. For example, including a linear combination of Slater determinants is possible as is modifying the orbitals to include spin correlations of backflow form [38]. Both of these avoid the exponential computational complexity, but may not capture the essential physics of the tensor force [39].

D. Path constraint

As in standard fermion diffusion Monte Carlo method, the AFDMC method has a fermion sign problem. The overlap of our walkers with the trial function will be complex in general, so the usual fermion sign problem becomes a phase problem.

To deal with this problem, we constrain the path of the walkers to regions where the real part of the overlap with our trial function is positive as in the original AFDMC paper [22]. We have also tried constraining the phase to that of the trial function as in the fixed phase approximation [40]. Both give about the same results, within error bars, and we report on the values where the real part is positive. For spin-independent time reversal invariant potentials, both reduce to the fixed-node approximation. It is straightforward to show that if the sign of the real part is that of the correct ground state, we will get the correct answer, and small deviations give second-order corrections to the energy. We have not been able to prove that this constraint always gives an upper bound to the ground-state energy although it appears to do so for the calculations we have done to date. It seems likely that there is not an upper bound theorem for the mixed estimate of the energy. A similar constraint used in GFMC calculations with full spin sums [41] was found to give an energy less than the ground-state value. While the operation of the constraint is somewhat different in the auxiliary field method, this further suggests that constraints of this sort do not give strict upper bounds. If forward walking or a path integral ground-state technique [42,43] is used, the method simply produces a better trial function, and the energy must be an upper bound.

In the fixed-node method [19] the nodal structure of the trial function is determined by the Slater determinant. Similarly, our path constraint is fully determined by the space spin Slater determinant of Eq. (38). The Jastrow function therefore affects only the variance and not our final results.

If perfect importance sampling with the correct propagator for our constraint were used, the walkers would never cross into a region with negative weight. However, with our short time approximations, we do get a small fraction of walkers that become negative and violate the constraint. These walkers are discarded as described below in Sec. IV F. The mistake made by discarding these walkers contributes to the time step error, and goes to zero as the time step error goes to zero. For a sample run, we found that for times steps of 1×10^{-5} MeV^{-1}, 2×10^{-5} MeV^{-1}, and 4×10^{-5} MeV^{-1} the absolute value of the ratio of the weight of the discarded walkers to the total weight is $(1.3\pm0.3)\times10^{-5}$, $(4\pm1)\times10^{-5}$, and $(10\pm1)\times10^{-5}$. Controlling the time step error therefore automatically controls this error. It should also be possible to modify the propagator in the vicinity of the constraint to properly go to zero as is often done in fixed-node calculations, but we have not done that here.

E. Tail corrections

Monte Carlo calculations are generally performed within the sphere of radius $L/2$, where L is the length of the box side. Usually, tail corrections are estimated by integrating out the spin-independent part of the two-body potential from $L/2$ up to infinity. We have made our calculations within the full simulation box, and, in order to also include the contribution from the neighboring cells, we have tabulated the Jastrow factor $f(r)$ and the components $v_p(r)$ of the two-body potential in the following form:

$$F(x,y,z) = \prod_{mno} f(|(x+mL_x)\hat{x} + (y+nL_y)\hat{y} + (z+oL_z)\hat{z}|),$$

$$V_p(x,y,z) = \sum_{mno} v_p(|(x+mL_x)\hat{x} + (y+nL_y)\hat{y} + (z+oL_z)\hat{z}|). \tag{39}$$

For the calculations shown, we found it adequate to include only the 26 additional neighbor cells corresponding to m, n, and o taking the values -1, 0, and 1.

Our results are therefore already tail corrected. We found that the standard way of treating tail corrections leads to results very close to ours, except when we consider model interactions which contain tensor forces, which are relatively long range forces.

The three-body potential is not treated as the two-body one. Here we have estimated the tail corrections to the three-body potential from the PBFHC variational results described in Sec. V. This analysis shows that such corrections are already very small for systems with 66 nucleons.

F. The algorithm

Finally, in this section we give the schematic structure of the AFDMC algorithm.

(1) Sample $|R,S\rangle$ initial walkers from $|\langle\Psi_T|R,S\rangle|^2$ using Metropolis Monte Carlo method.

(2) Propagate the spatial degrees of freedom in the usual diffusion Monte Carlo way with a drifted Gaussian for half a time step.

(3) For each walker, diagonalize the potential matrix (two- and three-body terms).

(4) Loop over the eigenvectors, sampling the corresponding Hubbard-Stratonovich variable, and update the spinors for half a time step. Introduce approximate importance sampling of the Hubbard-Stratonovich variables, as discussed at the beginning of Sec. IV.

(5) Propagate the spin orbit, using importance sampling.

(6) Repeat steps (2) –(4) in the opposite order to produce a reversible propagator to lower the time step error.

(7) Combine all weight factors and evaluate the new value of $\langle\Psi_T|R,S\rangle$. If the real part is less than 0, include the walker in the evaluation of the mixed and the growth energies, and then enforce constrained path by dropping the walker. In general, the importance sampling makes the number of dropped walkers small.

(8) Evaluate the averages of $\langle\Psi_T|R,S\rangle$ and $\langle\Psi_T|H|R,S\rangle$ to calculate the mixed energy.

(9) Repeat as necessary.

Note that with our choices for importance sampling and the auxiliary field breakup, we need to diagonalize the potential matrix and calculate the derivatives at each step. The additional computations to give the energy cost very little. To calculate error bars, block averages are calculated and the results combined over different block sizes until the blocks become uncorrelated and the error bars become independent of block size within statistics.

V. FHNC AND PBFHNC CALCULATIONS

In this section we present the method that we have used to estimate the finite size effects in AFDMC simulations. Such a method is made necessary by the fact that simulations with more than 100 nucleons are computationally very demanding. A many-body theory, such as FHNC, based on integral equation techniques, in which the number of particles in the simulation box has no practical limitation seems to be the best candidate to do this.

FHNC theory was originally developed [44–46] to treat fermionic systems in the thermodynamic limit. However, FHNC has been recently reformulated to deal with a finite number of fermions in a periodic box, as those used for the Monte Carlo calculations [29]. Such a theory, denoted as PBFHNC, is based upon the fundamental property of the FHNC cluster expansion to be valid at all $1/A$ orders [44–47], and it has been developed for Jastrow-correlated wave functions. In the cases of a nucleonic system interacting via a central potential, it has been shown that finite size effects are (i) not limited to the kinetic energy expectation value, and (ii) rather accurately estimated by PBFHNC calculations [25].

However, realistic correlations $\hat{F}(ij)$ are spin dependent and have an operational structure similar to that of the two-body potential, as in Eq. (2) (where the component $p=1$ corresponds to the Jastrow correlation). Therefore the PBFHNC developed in Ref. [29] cannot be used as such, but has to be generalized to treat spin-dependent correlations. The main problem is that the spin operators involved do not commute, namely, $[\hat{F}(ij),\hat{F}(ik)]\neq 0$. This feature makes a full FHNC summation impossible, and one has to resort to reasonable approximations for the spin-dependent correlations.

Such approximations are characterized by the fact that, whereas the cluster diagrams containing scalar correlations only are summed up with FHNC technique, only a limited set of cluster diagrams containing spin-dependent correla-

TABLE I. Variational parameters used in our FHNC/SOC and PBFHNC calculations for the $AU6'$ and $AU8'$ potentials. $r_0=[3/(4\pi\rho)]^{1/3}$ is the average distance between the neutrons. r_0, d_c, and d_t are given in fm. The reference density $\rho_0=0.16$ fm^{-3} is the equilibrium density of nuclear matter.

ρ/ρ_0	r_0	$d_c(6)$	$d_t(6)$	$a_s(6)$	$d_c(8)$	$d_t(8)$	$a_s(8)$
0.75	1.258	1.761	4.695	0.9	2.264	4.528	0.8
1.00	1.143	1.714	4.571	0.9	2.285	4.571	0.8
1.25	1.061	1.485	4.752	0.9	2.228	3.960	0.8
2.0	0.907	1.723	4.595	0.8	2.267	4.535	0.7
2.5	0.842	1.768	4.715	0.8	2.189	5.004	0.7

TABLE II. FHNC/SOC energy per particle of neutron matter for the $AU6'$ interaction, at various densities. T_F is the Fermi kinetic energy, and $\langle T\rangle$ is the kinetic energy expectation value, corresponding to the average of the JF and PB kinetic energies. $\langle V_2\rangle$ and $\langle V_3\rangle$ are the expectation values of the two-body and three-body potentials, respectively. ΔE_2 is the second-order perturbative correction [49]. $\Delta E_{\rm elem}$ is the contribution from the lowest order elementary diagram (see text). In the last column, $E_{\rm sum}$ is the sum of $E_{\rm FHNC}$, ΔE_2, and $\Delta E_{\rm elem}$. All the quantities, except ρ/ρ_0, are expressed in MeV.

ρ/ρ_0	T_F	$\langle T\rangle$	$\langle V_2\rangle$	$\langle V_3\rangle$	$E_{\rm FHNC}$	ΔE_2	$\Delta E_{\rm elem}$	$E_{\rm sum}$
0.75	28.969	35.33	−22.67	2.58	15.2	−0.9	0.6	14.9
1.00	35.094	43.82	−28.58	5.17	20.4	−0.9	0.9	20.4
1.25	40.722	52.27	−34.11	8.53	26.7	−1.5	1.2	26.4
2.0	55.708	74.40	−46.93	27.29	54.8	−4.4	2.8	53.2
2.5	64.643	88.85	−53.36	44.72	80.2	−6.1	3.8	77.9

TABLE III. Comparison of the FHNC/SOC results for the $AU8'$ interaction, obtained with correlation operator of the type f_6 or of the type f_8. In the first case the contribution of the spin-orbit potential is calculated perturbatively from the $AU6'$ Hamiltonian. For comparison, in the third column the results for the $AU6'$ interaction are also reported. In all cases the contribution from elementary diagrams has been added.

ρ/ρ_0	T_F	$AU6'$	$AU8'(f_6)$	$AU8'(f_8)$
0.75	28.969	15.8	16.1	13.3
1.00	35.094	21.3	21.8	17.6
1.25	40.722	27.9	28.8	23.0
2.0	55.708	57.6	59.0	47.5
2.5	64.643	84.0	86.2	71.7

tions are included in the calculation. The most tested and used approximation is the so called FHNC/SOC, described in Ref. [48]. In our calculations we have used the version adopted in Ref. [16] in order to compute the different correlation functions $\hat{F}(i,j)$ at the various densities considered. We have considered only the three variational parameters corresponding to healing distance d_c of central $(p=1-4)$ and spin-orbit correlations $(p=7,8)$, the healing distance d_t of tensor correlations $(p=5,6)$, and the quencher a_s of the spin-isospin–dependent correlation. The other variational parameters, such as the spin-independent potential quencher and the correlation quenchers, have been kept fixed at unity. The *optimal* values of such variational parameters for pure neutron matter are shown in Table I. They have been obtained by minimizing the average energy $E_{av}=(1/2)(E_{JF}+E_{PB})$, where the two energy expectation values E_{JF} and E_{PB} refer to the Jackson-Feenberg and Pandharipande-Bethe kinetic energy expressions, respectively [48]. The usual constraint $|E_{JF}-E_{PB}|/E_{av}\lesssim 0.005$ has been imposed in order to limit the range of variability of the free parameters in a region of reliability of the FHNC/SOC approximation. We have verified that in such region the normalization condition is fulfilled within a few percent.

The variational energies for the case of the $AU6'$ interaction are reported in Table II. The table also reports on the second-order CBF perturbative corrections ΔE_2 [49] and the contribution from the lowest order elementary diagram $\Delta E_{\rm elem}$, as discussed in Ref. [25]. The non-negligible value of $\Delta E_{\rm elem}$ indicates that the effect from elementary diagrams is larger than has been assumed in all the past FHNC/SOC calculations of the nuclear matter equation of state [25,28]. In recent FHNC/SOC calculations of the equation of symmetric nuclear matter and pure neutron matter [50,18] extra cluster diagrams with respect to the approximation used here have been included. Differences between the various FHNC/SOC calculations are within the predictive accuracy of the approximation.

TABLE IV. Comparison of the energy E_2 at the second order of the FHNC cluster expansion with the full FHNC energy $E_{\rm PBFHNC}$. The calculation has been performed for the v_6' model interaction at $\rho=0.16$ fm^{-3} and Jastrow correlation factor.

N	T_F	E_2	$E_{\rm PBFHNC}$
14	35.600	19.36	17.60
38	33.703	17.51	15.91
66	34.917	19.11	17.63
114	35.646	20.09	18.71
1030	35.139	19.46	18.04

TABLE V. PBFHNC/L results for the $AU6'$ interaction at density $\rho=0.16$ fm^{-3}. The Fermi kinetic energy T_F, the expectation values of the kinetic energy $\langle T\rangle$, the two-body potential $\langle V\rangle_2$ and the three-body potential $\langle V\rangle_3$ are displayed together with the energy per particle E in MeV units.

N	T_F	$\langle T\rangle$	$\langle V\rangle_2$	$\langle V\rangle_3$	E
14	35.600	44.47	−29.41	4.31	19.37
38	33.703	42.41	−29.43	4.70	17.68
66	34.917	43.64	−29.07	4.82	19.39
114	35.646	44.40	−28.87	4.87	20.40
1030	35.139	43.88	−28.95	4.86	19.79

In Table III we compare the results of two different FHNC/SOC calculations of the equation of state of neutron matter, carried out for the $AU8'$ potential. In the first one $[AU8'(f_6)]$ the spin-orbit correlation is set equal to zero, whereas, in the second one $[AU8'(f_8)]$, it is included. One can see that the introduction of the spin-orbit correlation leads to a large lowering in the energy. As it will be shown, we do not find such a lowering when the spin-orbit interaction is included in the AFDMC simulations. In the FHNC/SOC approximation the cluster contributions from spin-orbit correlations are correctly included only at the lowest order level. The many-body cluster contributions are essentially neglected. The large and attractive spin-orbit contribution found in the $AU8'(f_8)$ calculation may be due to this inaccuracy. On the other hand it might be possible that nodal surface induced by the spin-orbit part of the interaction is not accurately described by our trial function.

In order to compute the finite size effects in a realistic way, one should first generalize the PBFHNC theory to include SOC diagrams like in FHNC/SOC approximation. Work in this direction is in progress [51]. In this paper we limit ourselves to including only the two-body cluster diagrams for the two-body potential and the kinetic energy and the leading three-body cluster diagrams for the three-body

TABLE VI. As in Table V at density $\rho=0.32$ fm^{-3}.

N	T_F	$\langle T\rangle$	$\langle V\rangle_2$	$\langle V\rangle_3$	$\langle E\rangle$
14	56.512	74.33	−48.04	17.18	43.47
38	53.500	71.64	−50.25	19.36	40.75
66	55.428	73.41	−49.51	20.30	44.20
114	56.584	74.56	−48.94	20.78	46.40
1030	55.779	73.75	−49.08	20.84	45.51

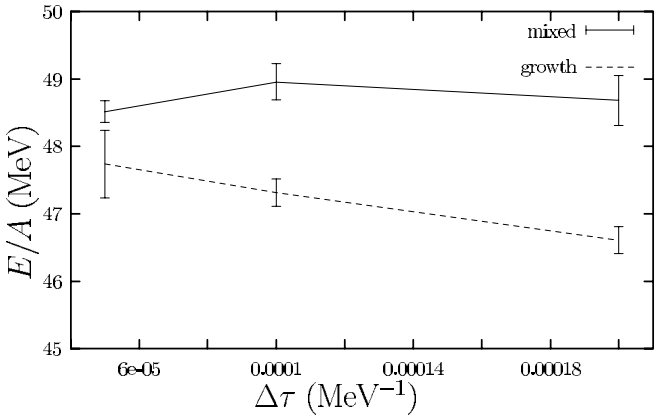

FIG. 1. Mixed and growth energies versus the time step for 14 neutrons at $\rho=0.32$ fm^{-3} with the $AU8'$ interaction.

potential [51] in the PBFHNC scheme. Such leading terms correspond to include up to two correlation operators in the three-body cluster diagrams. We will show that this approximation, hereafter denoted as PBFHNC/L, can already be used to roughly estimate the finite size effects.

The performance of the two-body cluster approximation to account for finite size effects is studied in Table IV. There, for a purely central correlation without three-body force, PBFHNC/L and PBFHNC energies are compared at $\rho=0.16$ fm^{-3} for the range of particle numbers used in our quantum Monte Carlo simulations.

Tables V and VI give the PBFHNC/L results for the $AU6'$ interaction at two different densities for a number of neutron systems. Note that the energy differences between the cases with 66 and 114 neutrons are very close to those obtained in the AFDMC simulations, given in Tables VIII and IX. Previous work [29] has shown that the PBFHNC results with 1030 particles are equal to the infinite system results to the accuracy shown. Systems with 14 and 38 neutrons are too small to be included easily in our simple finite size effects analysis. It may be possible to extrapolate from these very small simulations if sufficient care is taken. For example, the potentials may need to be more carefully cut off or summed, and the use of alternative boundary conditions is likely to be helpful [52]. Since larger system sizes are readily calculated with AFDMC, we simply increased the number of particles until the extrapolation became easier.

TABLE VII. AFDMC energies per particle in MeV of 14 neutrons in a periodic box for interaction models at various densities. Error bars for the last digit are shown in parentheses.

ρ(fm^{-3})	v_6'	v_8'
0.12	12.41(4)	12.32(5)
0.16	15.12(4)	14.98(6)
0.20	17.86(5)	17.65(7)
0.32	27.84(6)	27.3(1)
0.40	36.0(1)	35.3(1)

VI. RESULTS

A. AFDMC results for neutron matter

Extensive neutron matter calculations have been carried out for the $AU6'$ and $AU8'$ interactions by considering 14, 38, 66, and 114 neutrons in a periodic box at various densities ranging from $0.75\rho_0$ up to $2.5\rho_0$.

In Fig. 1 we show a typical behavior of the mixed and growth energy as a function the time step for 14 neutrons in a periodic box at $\rho=0.32$ fm^{-1} interacting via $AU8'$. At $\Delta\tau=5\times10^{-5}$ MeV^{-1}, we have found that the statistical error is smaller than the extrapolation ones, irrespective of the density and number of particles. All the calculations reported here have been obtained by using that value for the time step.

The 14-neutron system is interesting because it is small enough to be studied by using other many-body methods which become inefficient for larger systems. In order to provide a full set of results for this system in Table VII, we report on the energies at several densities calculated with the v_6' and v_8' interactions.

Diffusion Monte Carlo calculations using a pair-product wave function for 14-neutron systems have just been reported [28]. They, however, set the potential discontinuously to zero at distances greater than $L/2$, while we use either the nearest image convention or a lattice sum giving a continuous potential. We expect better extrapolation to large system sizes with the continuous potential as well as smaller time step errors. The time step errors will affect our AFDMC calculations more because we currently use the primitive approximation rather than building the Green's function from a product of exact two-body Green's functions. In principle, we could use the Hubbard-Stratonovich breakup for the pair-product Green's function. In any case, we have carried out a

TABLE VIII. AFDMC energies per particle in MeV for the $AU6'$ interaction obtained with systems with 14, 38, 66, and 114 neutrons at various densities. Error bars for the last digit of the Monte Carlo calculations are shown in parentheses. The last column gives the extrapolated values from the PBFHNC/L calculation [51].

ρ(fm^{-3})	AFDMC(14)	AFDMC(38)	AFDMC(66)	AFDMC(114)	AFDMC(∞)
0.12	14.96(6)	13.76(9)	14.93(4)	15.62(8)	15.0
0.16	19.73(5)	18.56(8)	20.07(5)	20.99(9)	20.4
0.20	25.29(6)	24.4(1)	26.51(6)	27.6(1)	26.9
0.32	48.27(9)	49.8(1)	53.11(9)	55.3(2)	54.4
0.40	69.9(1)	74.5(2)	79.4(2)	82.2(2)	81.3

TABLE IX. AFDMC energies per particle in MeV for the $AU8'$ interaction obtained with systems with 14, 38, and 66 neutrons at various densities. Error bars for the last digit of the Monte Carlo calculations are shown in parentheses. The last column gives the extrapolated values from the PBFHNC/L calculation [51].

$\rho(\mathrm{fm}^{-3})$	AFDMC(14)	AFDMC(38)	AFDMC(66)	AFDMC(∞)
0.12	14.80(9)	13.96(5)	15.26(5)	15.5
0.16	19.76(6)	18.67(6)	20.23(9)	20.6
0.20	25.23(8)	24.7(1)	27.1(1)	27.6
0.32	48.4(1)	46.8(2)	54.4(6)	55.6
0.40	70.3(2)	76.3(2)	81.4(3)	83.5

calculation at $\rho=0.16$ fm^{-3} using the same discontinuous potential, and obtained 20.64(2) MeV and 20.32(6) MeV for the v_6' and v_8' potentials, respectively, compared with their values of 19.91(11) and 17.00(27). The larger difference when the spin-orbit term is included in the Hamiltonian may be due to the different trial wave functions used.

In Tables VIII and IX we report on the results obtained with the AFDMC method of this work for neutron matter at the different densities considered for various system sizes. The extrapolation to infinite number of particles is carried out by using the PBFHNC/L results for a given number of neutrons and for the infinite system.

The spin-orbit contribution is rather small at all of the densities considered. This contrasts with previous FHNC/SOC calculations. In Fig. 2, we plot the AFDMC results together with the variational FHNC/SOC results for the v_8' interaction obtained by using correlation operators of the F_6 and F_8 forms, with the extrapolated unconstrained path Green's function Monte Carlo (GFMC-UP) of Ref. [28] from 14-neutron simulations with the v_8' interaction, and the Brueckner-Hartree-Fock (BHF) results for the v_{18} potential [53]. One can see that SOC($F6$) and SOC($F8$) in the figure give quite different equations of state, particularly at high densities.

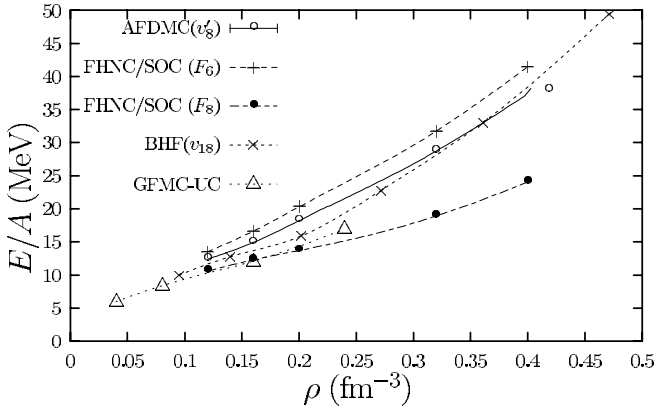

FIG. 2. AFDMC energy per particle for neutron matter from simulations with 66 neutrons and the v_8' potential. Variational FHNC/SOC results obtained with correlation functions of types F_6 and F_8 along with the the extrapolated unconstrained path GFMC-UP of Ref. [28] and the BHF results of Ref. [53]. The statistical errors in the AFDMC results are smaller than the symbols.

TABLE X. AFDMC energies per particle in MeV for the v_6' + IL potentials calculated with 66 particles. For the case of v_6' + IL2 interaction, at $\rho=0.32$ fm^{-3} the energies per particle with 38 and 54 neutrons are 12.6(2) and 10.0(3) MeV, respectively.

$\rho(\mathrm{fm}^{-3})$	$AU6'$	IL1	IL2	IL3	IL4
0.16	20.07(5)	11.2(1)	11.39(8)	12.0(4)	10.5(2)
0.32	53.11(9)	8.0(4)	11.1(3)	14.7(3)	4.7(3)

This difference in the effect of the spin-orbit potential in FHNC methods and AFDMC is quite different for the two techniques. We have tried including orbitals with spin-orbit correlations of a backflow form [39] which, while giving a lowering in the energy, does not resolve the discrepancy. Neither transient estimates nor these spin-backflow orbitals reduce the energy by more than roughly 5%. However, there is still a possibility that our constraining wave functions do not contain enough overlap with the correct spin-orbit induced states, and the transient estimates may not have been run for sufficient time to buildup the correct state. Like all transient methods, they are limited by the exponential buildup of noise.

The three-body potential gives a large contribution to the energy per particle at high densities. Therefore the search for a realistic three-body potential is a very fundamental problem for the study of dense and cold hadronic matter. A considerable amount of work has been done to find, in a semiphenomenological way, three-body potentials to describe ordinary matter. However, whether such potentials are also valid in the high density regime is still an open and debated issue. In Table X we report on AFDMC results performed with the two body v_6' interaction and five different three-body potentials including the Urbana-IX [12,20] (UIX) and the recent Illinois 1 through four [13] three-body interactions. One can see that already at twice the nuclear matter density, the energy contributions from the three-body poten-

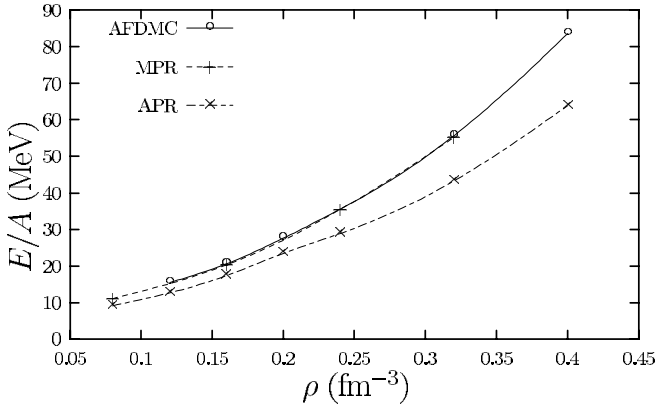

FIG. 3. Extrapolated AFDMC equation of state of pure neutron matter with the $AU8'$ potential (solid line). The variational results of Refs. [50] (APR, dotted-dashed line) and [18] (MPR, dashed line) corresponding to the Argonne v_{18} two-body plus Urbana-IX three-body potential are also plotted. The lines are for guiding the eyes. The statistical errors of the AFDMC estimates are smaller than the symbols.

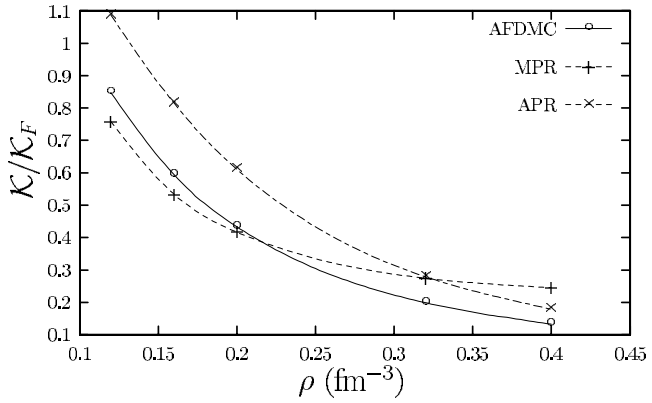

FIG. 4. Compressibility ratio $\mathcal{K}/\mathcal{K}_F$ for neutron matter obtained from the extrapolated AFDMC energy per particle with the $AU8'$ potential (solid line). The compressibility obtained from the variational results of Refs. [50] (APR, dotted-dashed line) and [18] (MPR, dashed line) is also plotted. The lines are for guiding the eyes. The statistical errors of the AFDMC estimates are smaller than the symbols.

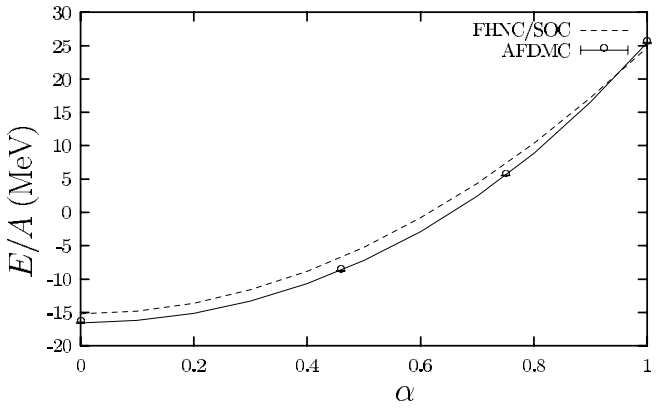

FIG. 5. AFDMC and FHNC/SOC energy per particle of nuclear matter for several values of the asymmetry parameter [25]. The lines correspond to polynomial fits of the calculated energies.

tials are large and very different from each other, in spite of the fact that all of them provide a satisfactory fit to the ground state and the low energy spectrum of nuclei with $A \leqslant 8$.

In Fig. 3 we show the AFDMC equation of state for pure neutron matter with the $AU8'$ interaction corresponding to the extrapolated values for infinite matter. We compare with the variational results of Ref. [50] and the more recent ones of Ref. [18]; both of them are obtained with the Argonne v_{18} two- and Urbana-IX three-nucleon interactions. One can see that there is a surprising accidental agreement between our AFDMC results and the latest variational calculation of Ref. [18].

The compressibility $\mathcal{K}$, given by

$$\frac{1}{\mathcal{K}} = \rho^3 \frac{\partial^2 E_0(\rho)}{\partial \rho^2} + 2\rho^2 \frac{\partial E_0(\rho)}{\partial \rho}, \tag{40}$$

can be estimated from the equation of state by taking $E_0 = E/A$. For a Fermi gas the compressibility is $\mathcal{K}_F = 9\pi^2 m/(k_f^5 \hbar^2)$. The AFDMC results for $\mathcal{K}/\mathcal{K}_F$ obtained from the extrapolated energies with $AU8'$ are shown in Fig. 4. They are compared with the compressibility calculated from the variational energies of Refs. [18,50].

TABLE XI. Finite size corrections for symmetrical nuclear matter [25]. PBFHNC results for the MS3 potential at $\rho = 0.16$ fm^{-3}. The PBFHNC calculations have been performed with a Jastrow-correlated wave function, whereas the FHNC/SOC result has been obtained with a correlation operator of the type F_4. PBFHNC and FHNC/SOC calculations include the basic four-point elementary diagram E_4.

A	PB-FHNC	FHNC/SOC	AFDMC
28	-13.6		$-16.17(6)$
76	-15.6		$-18.08(3)$
2060	-14.0		
∞	-14.0	-14.9	$-16.5(1)$

B. AFDMC results for nuclear matter

The AFDMC can deal with $N \neq Z$ systems, and we have applied it to compute the asymmetry coefficient of the mass formula for the semirealistic two-body potential MS3 which is spin-isospin dependent but has no tensor force [54,55]. The resulting values of E/A at ρ_0 for symmetrical nuclear matter are given in Table XI, where they are also compared with the FHNC/SOC and PBFHNC results. The finite size correction is estimated from the corresponding PBFHNC results.

In Fig. 5 we plot the AFDMC energy per particle as a function of the asymmetry parameter, $\alpha = (N-Z)/(N+Z)$, of nuclear matter. The FHNC/SOC curve corresponds to a quadratic fit of nuclear matter ($\alpha = 0$) and pure neutron matter ($\alpha = 1$).

FHNC/SOC can only be used to study $N = Z$ or $N = A$ matter. The symmetry energy obtained from FHNC/SOC is 41.59 MeV. The function $E/A(\alpha)$ provided by the AFDMC results is not fully quadratic in α, and corresponds to a symmetry energy of ~ 36.4 MeV.

VII. OUTLOOK AND CONCLUSIONS

We have described a quantum Monte Carlo method specially suited to perform calculations on nucleon systems with noncentral interactions. It has been applied here to calculate the equation of state of pure neutron matter with fully realistic interactions by approximating it with up to 114 neutrons in a simulation box. Finite size effects have been estimated by performing two- plus three-body cluster diagrams calculations based on PBFHNC method with spin-dependent correlations. The results obtained show an overall agreement with Brueckner–Hartree-Fock calculations and with a recent two- plus three-body cluster diagram variational calculation [18] with the exception of the spin-orbit effects in these latter calculations. Our results indicate that there is a very small contribution coming from the spin-orbit component of the two-body interaction while the effect from the three-body

potential is quite large, particularly at high densities. The large differences obtained for the equation of state for different phenomenological three-body potentials point out a three-body potential problem in the study of dense and cold hadronic matter.

Work in progress is to validate the present results using trial wave functions, other than the simple Slater determinant given in Eq. (38), which can also be calculated efficiently [39]. This will allow us to both lower the variance of our calculations, as is usual when better guiding functions are used in the importance sampling of the random walk, as well as to obtain a better path constraint.

We believe that our method should be able to produce accurate Monte Carlo calculations of a wide variety of nuclear systems. While previous Monte Carlo calculations have been severely restricted on the particle number by the spin-isospin sum, this restriction is lifted by using the auxiliary field breakup of the spin-isospin part of the Hamiltonian, while using standard diffusion Monte Carlo for the spatial degrees of freedom. A pressing need is simulating nuclear matter with fully realistic interactions as already done for pure neutron matter, calculating the properties of light nuclei to compare with exact GFMC calculations, and investigating pion condensation. In addition, including explicit meson degrees of freedom can also be attempted. In the language of this paper, each meson field mode corresponds to an auxiliary field [22].

ACKNOWLEDGMENTS

We wish to thank A. Fabrocini, V. R. Pandharipande, A. Polls, S. Pieper, and R. Wiringa for helpful discussions. S.F. wishes to thank the International Center for Theoretical Physics in Trieste for partial support. A.S. acknowledges the Spanish Ministerio de Ciencia y Tecnología for partial support under Contract No. BMF2002-00200.

[1] V.R. Pandharipande, I. Sick, and P.K.A. deWitt Huberts, Rev. Mod. Phys. **69**, 981 (1997).
[2] G.G. Raffelt, *The Stars as Laboratories of Fundamental Physics* (University of Chicago, Chicago, 1996).
[3] R.F. Sawyer, Phys. Rev. D **11**, 2740 (1975).
[4] R.F. Sawyer, Phys. Rev. C **40**, 865 (1989).
[5] N. Iwamoto and C.J. Pethick, Phys. Rev. D **25**, 313 (1982).
[6] S. Reddy, M. Prakash, J.M. Lattimer, and J.A. Pons, Phys. Rev. C **59**, 2888 (1999).
[7] R.B. Wiringa, V.G.J. Stoks, and R. Schiavilla, Phys. Rev. C **51**, 38 (1995).
[8] V.G.J. Stoks, R.A.M. Klomp, C.P.F. Terheggen, and J.J. de Swart, Phys. Rev. C **49**, 2950 (1994).
[9] R. Machleidt, F. Sammarruca, and Y. Song, Phys. Rev. C **53**, R1483 (1996).
[10] V.G.J. Stoks, R.A.M. Klomp, M.C.M. Rentmeester, and J.J. de Swart, Phys. Rev. C **48**, 792 (1993).
[11] L. Engvik, M. Hjorth-Jensen, R. Machleidt, H. Müther, and A. Polls, Nucl. Phys. **A627**, 85 (1997).
[12] B.S. Pudliner, V.R. Pandharipande, J. Carlson, and R.B. Wiringa, Phys. Rev. Lett. **74**, 4396 (1995).
[13] S.C. Pieper, V.R. Pandharipande, R.B. Wiringa, and J. Carlson, Phys. Rev. C **64**, 14 001 (2001).
[14] S.C. Pieper, K. Varga, and R.B. Wiringa, Phys. Rev. C **66**, 044310 (2002).
[15] A. Ramos, W.H. Dickhoff, and A. Polls, Phys. Rev. C **43**, 2239 (1991).
[16] R.B. Wiringa, V. Fiks, and A. Fabrocini, Phys. Rev. C **38**, 1010 (1988).
[17] A. Akmal and V.R. Pandharipande, Phys. Rev. C **56**, 2261 (1997).
[18] J. Morales, Jr., V.R. Pandharipande, and D.G. Ravenhall, Phys. Rev. C **66**, 054308 (2002).
[19] K.E. Schmidt and M.H. Kalos, in *Monte Carlo Methods in Statistical Physics*, edited by K. Binder (Springer-Verlag, Berlin, 1984), pp. 125–143.
[20] B.S. Pudliner, V.R. Pandharipande, J. Carlson, S.C. Pieper, and R.B. Wiringa, Phys. Rev. C **56**, 1720 (1997).
[21] S.C. Pieper, in *Microscopic Quantum Many-Body Theories and Their Applications*, edited by J. Navarro and A. Polls, Lecture Notes in Physics Vol. 510 (Springer-Verlag, Berlin, 1998), p. 337.
[22] K.E. Schmidt and S. Fantoni, Phys. Lett. B **446**, 99 (1999).
[23] S. Zhang, J. Carlson, and J.E. Gubernatis, Phys. Rev. Lett. **74**, 3652 (1995).
[24] S. Zhang, J. Carlson, and J.E. Gubernatis, Phys. Rev. B **55**, 7464 (1997).
[25] S. Fantoni, A. Sarsa, and K.E. Schmidt, in *Advances in Quantum Many-Body Theory*, edited by R.F. Bishop, K.A. Gernoth, and N.R. Walet (World Scientific, Singapore, 2001), Vol. 5, pp. 143–151.
[26] S. Fantoni, A. Sarsa, and K.E. Schmidt, Prog. Part. Nucl. Phys. **44**, 63 (2000).
[27] S. Fantoni, A. Sarsa, and K.E. Schmidt, Phys. Rev. Lett. **87**, 181101 (2001).
[28] J. Carlson, J. Morales, Jr., V.R. Pandharipande, and D.G. Ravenhall, preprint, nucl-th/0303041.
[29] S. Fantoni and K.E. Schmidt, Nucl. Phys. **A690**, 456 (2001).
[30] R.B. Wiringa, Argonne v_{18} and v_8' Potential Package, http://www.phy.anl.gov/theory/research/av18/av18pot.f (1994).
[31] R.B. Wiringa and S.C. Pieper, Phys. Rev. Lett. **89**, 182501 (2003).
[32] J. Carlson, V.R. Pandharipande, and R.B. Wiringa, Nucl. Phys. **A401**, 59 (1983).
[33] J. Lomnitz-Alder, V.R. Pandharipande, and R.A. Smith, Nucl. Phys. **A361**, 399 (1981).
[34] J. Carlson, Phys. Rev. C **38**, 1879 (1988).
[35] E. Buendía, F.J. Gálvez, J. Praena, and A. Sarsa, J. Phys. G **26**, 1795 (2000).
[36] J. Carlson and M.H. Kalos, Phys. Rev. C **32**, 2105 (1985).
[37] S. Zhang and H. Krakauer, preprint, cond-mat/0208340.
[38] S. Fantoni, in *Advances in Quantum Many Body Theories*, edited by A. Fabrocini, S. Fantoni, and E. Krotscheck (World Scientific, Singapore, 2002), Vol. 7, pp. 379–405.

[39] L. Brualla, S.A. Vitiello, A. Sarsa, S. Fantoni, and K.E. Schmidt, Phys. Rev. C **67**, 065806 (2003).
[40] G. Ortiz, D.M. Ceperley, and R.M. Martin, Phys. Rev. Lett. **71**, 2777 (1993).
[41] R.B. Wiringa, S.C. Pieper, J. Carlson, and V.R. Pandharipande, Phys. Rev. C **62**, 14 001 (2000).
[42] S. Baroni and S. Moroni, Phys. Rev. Lett. **82**, 4745 (1999).
[43] A. Sarsa, K.E. Schmidt, and W.R. Magro, J. Chem. Phys. **113**, 1366 (2000).
[44] S. Fantoni and S. Rosati, Nuovo Cimento Soc. Ital. Fis., A **10A**, 145 (1974).
[45] S. Fantoni and S. Rosati, Lett. Nuovo Cimento Soc. Ital. Fis. **10**, 545 (1974).
[46] S. Fantoni and S. Rosati, Nuovo Cimento Soc. Ital. Fis., A **25A**, 593 (1975).
[47] S. Fantoni and A. Fabrocini, in *Microscopic Quantum Many-Body Theories and Their Applications* (Ref. [21]), pp. 119–186.
[48] V.R. Pandharipande and R.B. Wiringa, Rev. Mod. Phys. **51**, 821 (1979).
[49] A. Fabrocini (private communication).
[50] A. Akmal, V.R. Pandharipande, and D.G. Ravenhall, Phys. Rev. C **58**, 1804 (1998).
[51] F. Arias de Saavedra, A. Sarsa, S. Fantoni, and K.E. Schmidt, (unpublished).
[52] C. Lin, F.H. Zong, and D.M. Ceperley, Phys. Rev. E **64**, 016702 (2001).
[53] M. Baldo, G. Giansiracusa, U. Lombardo, and H.Q. Song, Phys. Lett. B **473**, 1 (2000).
[54] I.R. Afnan and Y.C. Tang, Phys. Rev. **175**, 1337 (1968).
[55] R. Guardiola, in *Recent Progress in Many-Body Theories*, edited by J.G. Zabolitzky, M. de Llano, M. Fortes, and J.W. Clark, Lecture Notes in Physics Vol. 142 (Springer-Verlag, Berlin, 1981), pp. 398–406.